



Tunable free-electron X-ray radiation from van der Waals materials

Michael Shentcis¹✉, Adam K. Budniak², Xihang Shi¹, Raphael Dahan¹, Yaniv Kurman¹, Michael Kalina³, Hanan Herzig Sheinfux⁴, Mark Blei⁵, Mark Kamper Svendsen⁶, Yaron Amouyal³, Sefaattin Tongay⁵, Kristian Sommer Thygesen⁶, Frank H. L. Koppens^{4,7}, Efrat Lifshitz², F. Javier García de Abajo^{4,7}, Liang Jie Wong⁸ and Ido Kaminer¹✉

Tunable sources of X-ray radiation are widely used for imaging and spectroscopy in fundamental science, medicine and industry. The growing demand for highly tunable, high-brightness laboratory-scale X-ray sources motivates research into new fundamental mechanisms of X-ray generation. Here, we demonstrate the ability of van der Waals materials to serve as a platform for tunable X-ray generation when irradiated by moderately relativistic electrons available, for example, from a transmission electron microscope. The radiation spectrum can be precisely controlled by tuning the acceleration voltage of the incident electrons, as well as by our proposed approach: adjusting the lattice structure of the van der Waals material. We present experimental results for both methods, observing the energy tunability of X-ray radiation from the van der Waals materials WSe_2 , $CrPS_4$, $MnPS_3$, $FePS_3$, $CoPS_3$ and $NiPS_3$. Our findings demonstrate the concept of material design at the atomic level, using van der Waals heterostructures and other atomic superlattices, for exploring novel phenomena of X-ray physics.

The wealth of unique properties of van der Waals (vdW) materials in either bulk or single-atomic-layer form have constituted the basis of many novel physical phenomena and fundamental advances in recent years^{1–3}. For example, graphene, an atom-thick layer of graphite⁴, exhibits ultra-high carrier mobility at room temperature⁵, excellent optical transparency⁶, high Young's modulus⁷, high thermal conductivity⁸ and many other properties of practical utility. Moreover, this material has enabled the observation of novel phenomena such as the room-temperature quantum Hall effect⁹. Transition metal dichalcogenides (TMDs)^{10,11} and transition metal thiophosphates¹² have also emerged as intriguing families of vdW materials. Semiconductors by nature, TMDs can exhibit both an indirect bandgap in the bulk and a direct bandgap as a single atomic layer¹⁰. This unique property, combined with weak dielectric screening in two dimensions¹³, gives rise to strong photoluminescence and large exciton-binding energies, making TMDs attractive materials for light-emitting devices¹⁴. Likewise, transition metal thiophosphates are layered semiconductors additionally characterized by unique magnetic properties that make them potentially useful for application in quantum information devices and in spintronics¹⁵.

Here, we show how vdW materials can be used to explore novel phenomena of X-ray physics, in which free electrons passing through vdW layered structures create tunable X-ray radiation. Our findings thus present a new class of applications for vdW materials, as possible platforms for X-ray sources with a table-top footprint that have the advantages of being tunable and monochromatic relative to all existing compact sources. We demonstrate the unprecedented tunability of X-ray generation using free electrons passing through vdW

materials, and explore the processes by which the X-ray is generated, using both theory and experiments (Fig. 1a–c). The two mechanisms involved are parametric X-ray radiation (PXR) and coherent bremsstrahlung (CBS)^{16–19}. Both mechanisms arise simultaneously as a result of periodic interactions of free electrons propagating through an atomic structure (more detailed descriptions are provided at the beginning of the Results section).

In our experiment, the output photon energy is controlled by changing the incident electron energy, as well as through a method based on adjusting the composition and stacking of the vdW material structure. We present a comparative study demonstrating the highly precise dependence of the X-ray energy spectrum on the choice of the transition metal atom in the vdW material (iron (Fe), cobalt (Co) or nickel (Ni) as the 'X' in XPS₃). Looking at the big picture, the experimental results presented here constitute a proof of principle for our proposed wider design approach: to precisely tailor the radiation energy spectrum and angular distribution of X-ray emission by means of material design at the atomic level. We show that a wide range of superlattice crystalline materials, both natural and artificial, can be used for X-ray generation, and we present a theory for X-ray emission from designed superlattice structures. These findings pave the way towards the use of superlattice atomic structures for realization of tunable and versatile sources of X-ray radiation with a table-top footprint.

The appeal of using vdW materials for X-ray generation is enhanced by the fact that many vdW materials possess high in-plane thermal conductivities²⁰, and some have higher melting temperatures than conventional materials. Moreover, radiation damage can be further reduced by using heterostructures combining different

¹Department of Electrical Engineering, Technion—Israel Institute of Technology, Haifa, Israel. ²Schulich Faculty of Chemistry, Technion—Israel Institute of Technology, Haifa, Israel. ³Department of Materials Science and Engineering, Technion—Israel Institute of Technology, Haifa, Israel. ⁴ICFO—Institut de Ciències Fotoniques, The Barcelona Institute of Science and Technology, Castelldefels, Spain. ⁵School for Engineering of Matter, Transport and Energy, Arizona State University, Tempe, AZ, USA. ⁶CAMD and Center for Nanostructured Graphene (CNG), Department of Physics, Technical University of Denmark, Kongens Lyngby, Denmark. ⁷ICREA—Institut Català de Recerca i Estudis Avançats, Barcelona, Spain. ⁸School of Electrical and Electronic Engineering, Nanyang Technological University, Singapore, Singapore. ✉e-mail: michael.shentcis@gmail.com; kaminer@technion.ac.il

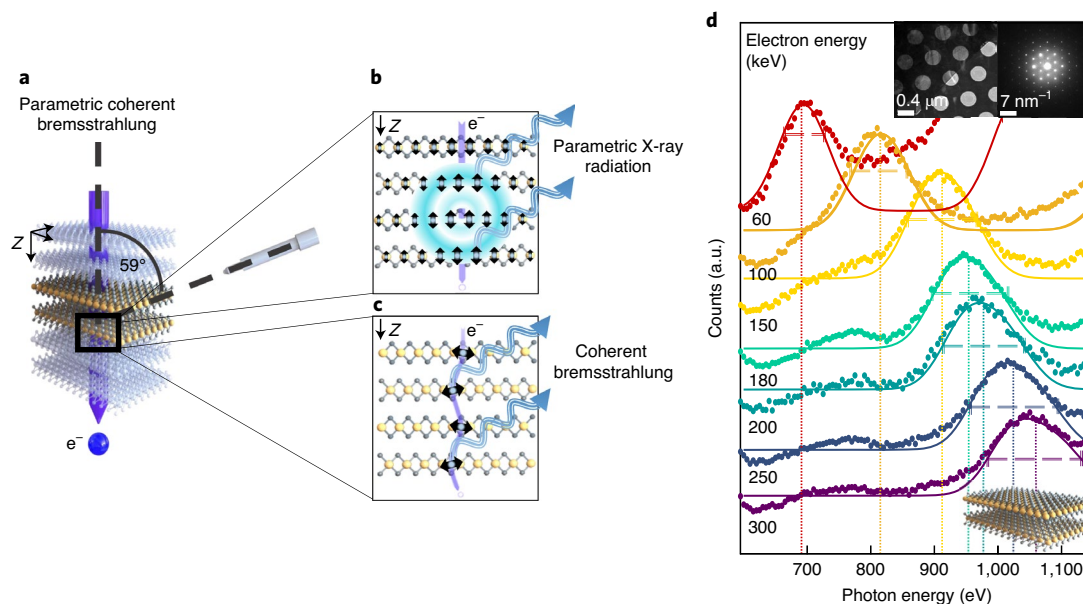


Fig. 1 | Demonstration of free-electron radiation from vdW materials. **a**, The radiation is produced from two combined mechanisms, PXR and CBS, both emitted with the same dispersion relation (equation (1)) from an electron (e^-) propagating through periodic crystal structures (aligned along the Z axis). The angle between the direction of the detector and the negative direction of electron propagation is 59° . **b**, Illustration of the PXR mechanism, produced as the particle's electromagnetic field (light blue halo) is diffracted off the periodic crystal structure. **c**, Illustration of the CBS mechanism, describing the X-ray emission by an undulated electron due to a series of periodic bremsstrahlung interactions with the crystal lattice. **d**, Photon energy spectrum of X-ray radiation created by an electron moving along the [001] zone axis of WSe_2 . The emitted radiation peaks at different photon energies, depending on the electron kinetic energy (60–300 keV). The experimental results (dotted curves) are in good agreement with the theoretical prediction both for the peak energy (equation (1) with $m = 2$, vertical dotted lines) and the peak width (equation (2), horizontal dashed lines), using no fitting parameters. We compare the results with simulations of PXR and CBS and present the PXR theory that is found to be stronger in this case (solid curves). The trends match the experimental observation, with the only fitting parameters being the y axis scaling of each curve. We attribute deviations of the experimental results from the simulated curves to emission from core transitions (a broad peak around ~ 780 eV and on the right edge). Insets: sample image and diffraction pattern (top right); 3D model (bottom right). a.u., arbitrary units.

kinds of vdW materials^{21,22}. Other qualities are specifically attractive for PXR and CBS and arise from the weak bonding between the layers in vdW materials, which helps to maintain the crystalline nature of the material that is crucial for both mechanisms. Moreover, the crystal structures of vdW materials are characterized by larger unit cells than those of conventional three-dimensional (3D) bulk crystalline materials. As shown below, the larger unit cell enables X-ray generation with relatively high brightness in spectral ranges such as the water window (useful for biological imaging²³), using electron energies obtainable from laboratory-scale electron sources such as those used in transmission electron microscopes (TEMs) and scanning electron microscopes (SEMs). Furthermore, the wide range of compositions and flexibility in the stacking of vdW materials provide extra tunability to shape the output radiation through controlling the atomic lattice geometry.

Energy tunability of X-ray sources is a key factor in many applications, such as core-level spectroscopy^{24–26} and various X-ray imaging techniques^{27–29}. The energy tunability required for such applications is usually achieved in undulator facilities, such as synchrotrons and free-electron lasers^{30–32}. However, the operation of such facilities necessitates immense resources in terms of space, energy and safety measures, which limit their accessibility. Most laboratory-scale sources take the form of an X-ray tube, in which free electrons are used to induce bremsstrahlung or core transitions that produce X-rays. Such sources do not provide energy tunability or radiation directionality capabilities, which have a lot of potential for a wide variety of uses.

These limitations motivate research into new physical mechanisms for X-ray generation with the potential to create

laboratory-scale X-ray sources that are tunable and directional. In particular, research advances in X-ray-generation mechanisms have led to the development of laser-driven Compton-based X-ray sources³³ that use the micrometre-scale periodicity of light, which is much smaller than the millimetre/centimetre scales of conventional undulator facilities. Such smaller-scale undulators enable the levels of electron acceleration to be reduced, while still resulting in tunable X-ray generation. More recent proposals rely on shrinking the undulating periodicity even further by leveraging the high electromagnetic confinement in graphene surface plasmons³⁴, metasurfaces³⁵, metamaterials³⁶ and nanophotonic vacuum fluctuations³⁷. Our study explores different phenomena that lead to X-ray generation from free electrons, in which the electron undulation is done at the ultimate periodicity: that of the atomic crystal lattice.

Results

Tunable X-ray radiation from vdW materials. The vdW-material-based atomic undulator that we present here relies on two radiation mechanisms, CBS and PXR, using modest electron energies that are available in relatively simple systems such as a TEM. The mechanisms of CBS and PXR have not yet been studied in vdW materials. Both mechanisms take place as a propagating electron undergoes coherent interaction with the intrinsic periodicity of a crystalline material (Fig. 1).

PXR is emitted from the modulation induced by the incident electron on the bound electrons of the material's atoms, creating polarization currents from which directional X-ray radiation is emitted. The PXR mechanism can also be described as diffraction of the incident electron's Coulomb field off the periodical atomic

arrangement of the structure (Fig. 1b). We model PXR by treating the periodic atomic structure as a discrete dipole array (described by the black arrows in Fig. 1b), with bound electrons around each atom being modelled as an effective dipole quantified through an associated X-ray atomic polarizability.

CBS is emitted from the incident electron as a result of a periodic series of bremsstrahlung interactions with the nuclei and bound electrons in the material, where each interaction involves acceleration of the electron, causing it to emit radiation (Fig. 1c). The modulation of the free-electron velocity by the periodic potential results in interference of the emitted radiation and causes it to become directional. We model CBS by considering the far-field radiation from electrons whose trajectories are calculated by using the relativistic Newton–Lorentz equations in the presence of an atomic potential, which is in turn obtained from density functional theory (DFT; Methods). We can equivalently describe the CBS emission by using a propagating radiating dipole excited as a result of the field induced by the electrons of the crystal structure (described by the black arrows in Fig. 1c).

The radiation emitted from each electron through the CBS and PXR mechanisms maintains temporal and spatial coherence (in contrast to coherence from multiple electrons, which requires bunching of the electrons). That is, the radiation emitted from multiple locations along the trajectory of the incident electron interferes constructively to produce angle-dependent output radiation (coherent interference from multiple locations is possible because the final quantum state of the material is not changed). The radiation from both mechanisms follows the same dispersion relation¹⁹

$$E_m = \hbar\omega_m = m \frac{2\pi\hbar c\beta \cos(\theta)}{d(1-\beta\cos(\varphi))} \quad (1)$$

where $\beta = v/c$ is the normalized speed of the electron (where v is the velocity of the electron and c is the velocity of light); E_m and ω_m are the photon energy and angular frequency, respectively, corresponding to radiation of order m (where $m = 1, 2, 3, \dots$); \hbar is the reduced Planck constant; d is the lattice constant; and θ and φ are the angles defining the electron velocity relative to the reciprocal lattice of the crystal and the photon emission direction, respectively.

Each of the PXR and CBS mechanisms becomes of greater influence at different regimes of emission energies and angles. However, they both share the same dispersion relation (equation (1)), and thus they can be effectively considered as a single combined effect^{38,39}, which we refer to as parametric coherent bremsstrahlung (PCB).

The unique structure and large variety of vdW materials make them promising candidates for PCB radiation for several reasons. One reason arises from the unique layered structure of vdW materials, which are made of strong covalently bonded atomic layers joined together by vdW forces. Consequently, the effect of integrating certain atoms (for example, tungsten) into a vdW structure (for example, WSe₂) can be seen as effectively ‘stretching’ the lattice constant d , thus redshifting the radiation energy peaks E_m . For example, the lattice constant of bulk tungsten, 3.16 Å, is increased to 12.98 Å (unit cell size in an AB stacking, that is, the distance between two alternate layers) when it is embedded into a WSe₂ TMD structure, giving rise to PCB X-ray radiation with a different energy–angle profile for the same incident electron velocities (Fig. 1d). The longer effective period of the vdW crystal allows soft X-ray photons (for example, in the water window) to be created with higher incident electron energy than in regular 3D bulk crystals—seen by the trade-off of d and β in equation (1). This regime of parameters leads to higher output power and brightness when using electrons from TEMs and SEMs.

Figure 2a,b presents PCB radiation from additional vdW structures, namely, MnPS₃ and CrPS₄, oriented along the [103] and [001] zone axes, respectively. As in Fig. 1d, we note a good agreement of the experimental results with the predicted energy values calculated from equation (1).

Using the PCB theory, we also predict the width $\Delta\omega$ of the spectral peaks, which for thin TEM samples and highly directional electron beams yields (Supplementary Section 1)

$$\frac{\Delta\omega}{\omega_m} = \frac{\Delta E}{E_m} \approx \sqrt{0.8 \frac{d^2}{m^2 L^2} + \Delta\varphi_D^2 \frac{\beta^2 \sin^2 \varphi}{[1-\beta\cos\varphi]^2} + \Delta\theta_e^2 \tan^2 \theta} \quad (2)$$

with ΔE being the energy width, L the electron interaction length in the crystal, $\Delta\varphi_D$ the angular aperture of the detector and $\Delta\theta_e$ the angular spread of the incident electron beam. In the present study, the width of the spectral lines is primarily determined by the angular aperture of the energy-dispersive X-ray spectrometer, 16°, which collects the emission for a range of angles $\varphi = 113^\circ$ – 129° . In contrast, the left term in the square root of equation (2) is comparatively negligible in our case because the crystal thicknesses of the different materials ($L \approx 100$ nm) do not introduce notable broadening relative to the angular aperture of the detector. Similarly, $\Delta\theta_e < 0.1$ mrad, estimated to be the electron beam divergence angle in our experiment, is small and does not substantially alter $\Delta\omega$. An additional effect of considerable broadening is the detector energy resolution (~ 80 eV), which has to be combined with the result of equation (2) (Methods).

We can use equation (2) to estimate the monochromaticity of the emitted radiation in a way that is independent of the detector parameters. Neglecting $\Delta\varphi_D$, we find that PCB radiation generated by a collimated electron beam results in $\Delta\omega/\omega_m = 0.9d/mL$, which means $\frac{1.2}{m}\%$ for an interaction length of 100 nm in WSe₂. Therefore, when collected over a small angle, the X-rays produced are indeed very monochromatic, possessing a narrow bandwidth below 1% for $m \geq 2$.

The positions of the experimental peak maxima in Figs. 1d and 2a–c show small deviations from the theoretical values (marked by vertical dotted lines), possibly due to small uncertainties in the detector angle or in the reported values of the interlayer distances used here as input parameters. Additional effects that explain deviations between theory and experiment include the background of incoherent bremsstrahlung radiation, different interaction lengths for each incident electron energy, divergence of the incident electron beam and further subsequent diffraction of the radiation by the crystal and the detector (Supplementary Section 7). The last effect should be sensitive to the properties of the electron beam because it essentially consists of Kossel-line-like diffraction from a coherent source comprising the emission from all of the atoms exposed to each incident electron wave. Additionally, our PXR simulation shows that since the detector is located in the backward direction relative to the electron velocity, there is a small Doppler shift that causes the energy peak to be slightly redshifted, in qualitative agreement with our measurements (seen in the theory and experiments in Fig. 1d).

We use the simulation tools here developed for CBS and PXR to quantify both mechanisms and compare them with our experimental results. We find that in our regime of interest (moderately relativistic electrons available from TEMs), the PXR mechanism dominates the radiation emission as it is two orders of magnitude larger than CBS. These models enable the average brightness values of PCB radiation sources from vdW materials to be theoretically predicted. For example, we examine the brightness values obtainable in a TEM set-up such as that used in this work: a relatively low electron current of ~ 1 nA and a ~ 1 nm electron beam diameter (at the plane of the sample) passing through a WSe₂ sample of ~ 100 nm thickness. For the detector orientation of $\varphi = 121^\circ$ with respect to the electron velocity, we estimate a brightness value of $\sim 1 \times 10^9$ photons s^{-1} mrad⁻² mm⁻² 0.1%BW⁻¹ within our range of energy tunability of ~ 700 – $1,100$ eV (where BW is the bandwidth). This level of brightness compares favourably with state-of-the-art X-ray tubes, while the input power is smaller by a factor of 10^{-5} – 10^{-8} (because

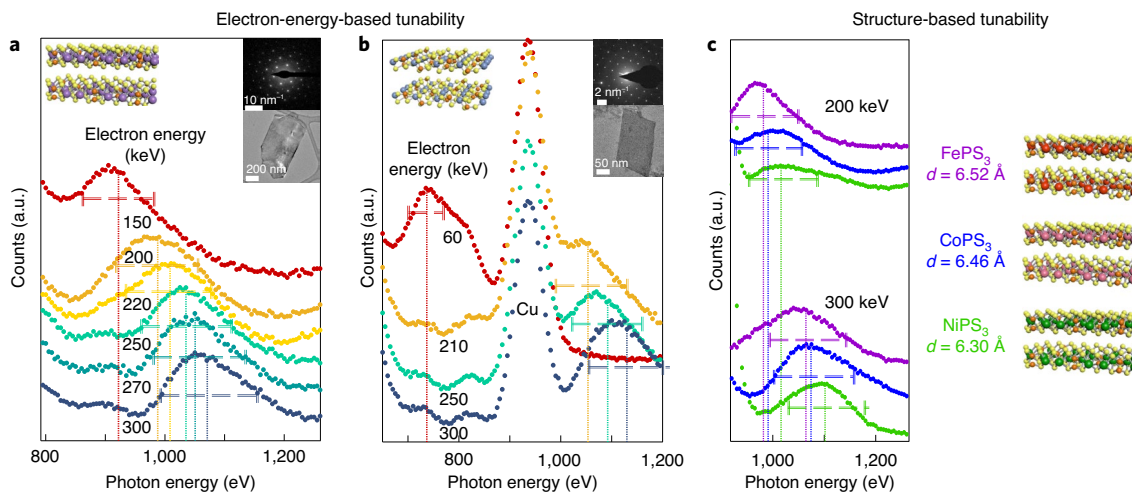


Fig. 2 | Tunability of X-ray radiation from vdW materials. **a, b**, X-ray radiation spectra collected from MnPS_3 (**a**) and CrPS_4 (**b**). The photon energy peak is tuned by varying the incident electron kinetic energy in the range 60–300 keV, as indicated. Theoretically predicted peak energy (equation (1) for $m=2$, vertical dotted lines) and peak width (equation (2), horizontal dashed lines) both show a good match with the experimental results. The constant energy peak in **b** is the characteristic radiation peak emitted from copper (Cu). Top right insets: sample image and diffraction pattern for crystal orientations of [001] (CrPS_4) (**b**) and [103] (MnPS_3) (**a**). Top left insets: 3D models of the layered vdW structures. **c**, Radiation from three vdW materials with the same crystal structure (FePS_3 (purple), CoPS_3 (blue) and NiPS_3 (green)), but differing by a picometre-scale difference in d (right inset). The resulting radiation energy tuning through structural modification is demonstrated at two incident electron kinetic energies, showing the possibility for combined X-ray energy tunability via variation of the structure and of the electron acceleration voltage. Sensitivity of the photon energy tuning is high, being limited only by the energy resolution and angular aperture of the detector. a.u., arbitrary units.

the electron spot diameter in our experiment is much smaller than that of X-ray tubes). Moreover, our PCB radiation is directional and tunable, in contrast to the radiation from X-ray tubes (which is either characteristic or bremsstrahlung). The estimated numbers of photons collected at the solid angle of the detector are $4.0 \times 10^3 \text{ photons s}^{-1} \text{ eV}^{-1}$, $2.6 \times 10^3 \text{ photons s}^{-1} \text{ eV}^{-1}$, $1.8 \times 10^3 \text{ photons s}^{-1} \text{ eV}^{-1}$, $1.5 \times 10^3 \text{ photons s}^{-1} \text{ eV}^{-1}$, $1.4 \times 10^3 \text{ photons s}^{-1} \text{ eV}^{-1}$, $1.1 \times 10^3 \text{ photons s}^{-1} \text{ eV}^{-1}$ and $1.0 \times 10^3 \text{ photons s}^{-1} \text{ eV}^{-1}$, at each peak from 60 keV to 300 keV (Fig. 1d and Methods). The typical number of photons per second is $\sim 10^5$ (integrating over the widths of the peaks).

The brightness of the PCB source can be further improved by optimizing parameters such as the detector orientation and size, the electron acceleration voltage and the sample thickness (similarly to other undulation-based emission mechanisms, the PCB brightness is quadratic with the interaction length). It can also be increased by using larger currents and reducing the electron spot size, for which an optimum compromise can be found by keeping in mind the trade-off enforced by Coulomb repulsion (space charge), which leads to greater beam divergence (hence smaller interaction length) with larger electron density. When the electron beam divergence exceeds about 0.1° , the heights of the radiation peaks start to broaden and decrease notably ($>5\%$ from their original values). When considering space charge, we show in Supplementary Fig. 5 that the potential increase in brightness of PCB from vdW materials can be as much as 10^7 times the value reported above (for an optimal combination of electron current and beam size).

The X-ray generation from the PCB mechanism can be extended to the hard X-ray regime with higher electron energies, as we show in Supplementary Section 4, where we simulate the output radiation from 1 MeV and 5 MeV electrons. Electron beams generated by relatively compact sources such as photoemission injectors based on radio-frequency guns and d.c. high-voltage guns^{40,41} enable higher electron currents of up to tens of milliamperes in acceleration voltages of a few megaelectronvolts, which can strongly improve the emission brightness from thicker crystal samples.

The performance of PCB radiation from vdW materials can also be viewed from the perspective of energy transfer and efficiency. The total probability of each 60 keV electron going through a 100 nm interaction length in WSe_2 to produce PCB emission is $\sim 1 \times 10^{-4}$, resulting in an average electron energy loss to PCB of 0.25 eV. Out of this, the probability of radiation in the direction of the detector is $\sim 1 \times 10^{-5}$, that is, electron energy loss to ‘useful X-ray photons’ of 0.025 eV. This probability is of the same order of magnitude as is found in related processes such as Smith–Purcell radiation. The efficiency can be further improved because the electron energy can be reused. Such an approach is used in many free-electron-based applications, such as travelling-wave tubes. Recycling the electron energy means that the absolute efficiency depends on competing channels of energy loss in the sample. In the case of PCB radiation, such processes mainly come from Coulomb collisions that result in the ionization of other electrons, excitation of atoms and non-coherent bremsstrahlung radiation. We use a numerical simulator developed by the National Institute of Standards and Technology to estimate the total energy loss of a 60 keV electron in a 100 nm sample from our materials, and find an average energy loss of ~ 300 eV. Therefore, we predicted the efficiency of the mechanism to be $\sim 0.1\%$ (60 keV electrons, 100 nm WSe_2).

At higher energies, the efficiency improves as the radiation is more directional due to relativistic contraction. In addition, higher electron energies have longer penetration depths in thicker samples (that is, lower competing loss channels). Overall, such efficiency can be tolerable when considering that X-ray sources are never generally efficient and bearing in mind that unlike any other compact X-ray source, PCB-based sources are tunable.

Discussion

We now discuss methods to control the emitted spectra from PCB radiation. The X-ray energy is tuned in Figs. 1d and 2a,b by adjusting the incident electron energy. However, such a method necessitates realignment to ensure that different conditions, such as the quality of the electron beam collimation, remain unchanged, thus adding a degree of difficulty to that approach. Another method for

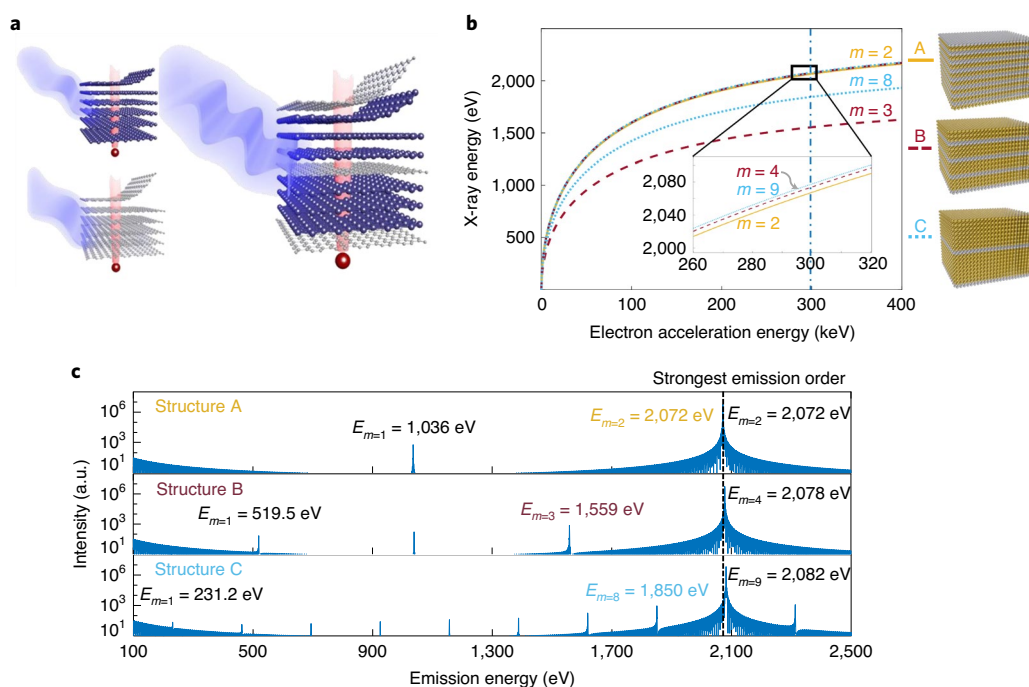


Fig. 3 | Spectral shaping of X-ray radiation via customized superlattices. **a**, Illustration of the proposed design concept for tuning PCB X-ray radiation energy, combining two crystalline materials into a heterostructure whose periodicity is customized by the choice of layers; vdW stacking and molecular beam epitaxy provide possible approaches to these heterostructures. **b**, X-ray emission peak energy of superlattice structures formed by alternating layers of graphite ($d_1 = 0.3350$ nm) and hexagonal boron nitride ($d_2 = 0.3308$ nm), used as an illustrative example. Each superlattice contains a different number of layers from each material, as shown in the models on the right: $n_1 = 1, n_2 = 1$ (structure A, yellow line); $n_1 = 1, n_2 = 3$ (structure B, red dashed line); $n_1 = 1, n_2 = 8$ (structure C, blue dotted line). The different choice of superlattice enables direct control over the number and energy of the resulting emission peaks. The choice of different emission orders enables coarse or fine energy tunability, as demonstrated in the plot and inset, respectively. **c**, Full emission spectra simulated under the conditions indicated by the vertical blue dashed-dotted line in **b** (300 keV kinetic energy), showing that the most dominant order of emission for each structure is $m = n_1 + n_2$ (see equation (3)). a.u., arbitrary units.

adjusting the output photon profile involves changing the orientation of the crystal with respect to the electron beam, which, unfortunately, compromises the emission efficiency and other properties of the output radiation.

Taking a different approach, we present in Fig. 2c the results of our method for controlling the output radiation spectra by precise manipulation of the lattice structure. Using several vdW materials with similar basic structures in which the main element is altered, we show that the resulting small but precise changes in the lattice constant lead to corresponding precision control over the spectral peaks of the emitted PCB radiation. Figure 2c shows three vdW materials sharing the formula XPS₃, where ‘X’ represents the transition metals Fe/Co/Ni. The lattice constant differs slightly between these vdW compounds (Fig. 2c, right inset), enabling fine energy tuning of the emission through lattice variation. This tuning method provides an extra handle of versatility on top of the conventional PCB tuning mechanisms of electron energy and orientation, further supporting the potential of vdW materials as compact platforms for high-quality X-ray generation.

Tunability by the structural design of vdW materials is the first step towards our proposed broader design concept, in which a specially engineered superlattice structure can be used to spectrally shape the emitted X-ray radiation. Analogous structural customizations for manipulating radiation have been suggested for other applications at optical wavelengths in metasurfaces⁴² and in designer Smith–Purcell gratings^{43,44}. However, this approach has never been considered for X-ray radiation manipulation.

Figure 3a presents our design approach by exploring a general superlattice configuration in which two crystalline materials are

combined into a superlattice. Mathematically, we derive a corrected dispersion relation where the lattice factor d in equation (1) is replaced by a weighted sum of lattice factors $d_1 n_1 + d_2 n_2$, with d_1 and d_2 denoting the lattice constants and n_1 and n_2 the number of layers in each period of the two combined crystals. We thus have (generalizing equation (1))

$$E'_m = \hbar\omega'_m = m \frac{2\pi\hbar\beta\cos\theta}{(d_1 n_1 + d_2 n_2)(1 - \beta\cos\theta)} \quad (3)$$

PCB radiation from monocrystalline materials is usually strongest for the first emission order ($m = 1$). However, in superlattices made of two materials, the dominant emission would occur at $m = n_1 + n_2$ (the total number of layers in a single superlattice period).

Figure 3b,c shows that changing the atomic composition of the superlattice period allows us to control the range of emitted radiation energy for the same incident electron velocities. The curves in Fig. 3b are calculated by combining graphite ($d_1 = 0.3350$ nm) and hexagonal boron nitride ($d_2 = 0.3308$ nm) into a superlattice structure and presenting several emission orders of such structures. The theoretical estimate of the intensity relation between emission orders in Fig. 3c is based on a model that uses a one-dimensional array of radiating dipoles. In this model, each dipole represents a lattice plane of the superlattice. As the PCB energy profile is dependent on the constructive interference of emission from consecutive lattice planes, we can calculate the relation between the emission peaks by considering the electromagnetic field emitted from a row of point dipoles with the corresponding relative phases. We note an excellent match between the emitted energies presented in this model and the dispersion relation in equation (3).

Outlook

We envision the use of vdW heterostructures^{45,46} and other artificial superlattice crystalline materials to optimize the emission of PCB X-ray radiation with user-defined spectral and spatial properties. These sources are also attractive due to practical considerations, such as the promise of higher stability and smaller dependence on recalibrations and electron beam alignments, because it is possible to tune the emission by changing between a series of superlattices without modifying the electron beam properties. Fabrication of such superlattice–PCB sources can benefit from a variety of new crystal growth techniques, as well as the large wealth of possible chemical compositions and crystal structures offered by vdW materials. Additionally, molecular beam epitaxy⁴⁷, metal organic chemical vapour deposition⁴⁸ and other established material-growth techniques could be used to enable superlattice design incorporating other material families (for example, III-Vs, II-VIs) for X-ray generation and manipulation.

Another meaningful improvement would be the use of nano-modulated electrons that could make the radiation coherent from multiple electrons (microbunching). These nano-modulated electrons can be generated via emittance exchange techniques^{49,50}, laser–plasma interactions⁵¹ or electromagnetic intensity gratings⁵². Future work could develop structures that achieve resonant PCB conditions for interaction between the propagating electrons and periodic structure to improve the emission efficiency of PCB radiation.

Our theoretical and experimental results show the advantages of vdW materials in engineering the emission of energy-tunable X-ray radiation. VdW materials add versatility to X-ray energy tuning of PCB radiation based on our proposed lattice modification technique, which can be combined with previously explored tuning techniques or used as a separate method. Additionally, this technique demonstrates the advantages of designer superlattices for energy-tunable emission of monochromatic and directional X-ray radiation.

In contrast to state-of-the-art tunable X-ray sources, PCB radiation can be generated from modestly relativistic electrons. This makes the superlattice–PCB X-ray sources relatively compact and more accessible for various applications, such as X-ray spectroscopy^{24–26}. For example, PCB radiation from vdW materials can be used for compact and tunable X-ray photoemission spectroscopy methods. Such an application is already within reach, using the emission flux and brightness of PCB from the low current of a basic TEM set-up, as described above.

Additional research tools such as transmission X-ray microscopy and scanning photoelectron microscopy⁵³ are also potential applications for future PCB sources. X-ray imaging techniques can benefit from the use of energy-tunable sources, as the image contrast is affected by the energy of the incident radiation^{27–29}. This concept may be used, for instance, to improve the yield and accuracy of mammography techniques, in addition to reducing the radiation dose delivered to a patient²⁸. Future imaging techniques that use the tunability of superlattice–PCB X-ray sources can create compact variants of K-edge imaging techniques⁵⁴ with limited brightness and flux, yet at accessible laboratory scales.

In conclusion, we theoretically predict and experimentally demonstrate tunable, high-brightness X-ray emission from vdW materials when irradiated by moderately relativistic electrons available, for example, from a TEM. The radiation spectrum can be precisely controlled by tuning the acceleration voltage of the incident electrons, as well as by our proposed approach—adjusting the lattice structure of the vdW material. We present experimental results for both methods, observing the energy tunability of X-ray radiation from the vdW materials WSe₂, CrPS₄, MnPS₃, FePS₃, CoPS₃ and NiPS₃. Our findings demonstrate the concept of material design at the atomic level, using vdW heterostructures and other atomic superlattices, for exploring novel phenomena of X-ray physics. Looking forward,

the control of atomic layers in both the longitudinal and transverse directions would enable spatial, angular and spectral shaping of output X-ray radiation. We envision the customization of superlattices for user-specific applications via inverse design techniques that optimize the desired output radiation characteristics, given the electron beam conditions and the specific geometrical constraints.

Online content

Any methods, additional references, Nature Research reporting summaries, source data, extended data, supplementary information, acknowledgements, peer review information; details of author contributions and competing interests; and statements of data and code availability are available at <https://doi.org/10.1038/s41566-020-0689-7>.

Received: 29 December 2019; Accepted: 7 August 2020;

Published online: 14 September 2020

References

- Novoselov, K. S. et al. Two-dimensional atomic crystals. *Proc. Natl Acad. Sci. USA* **102**, 10451–10453 (2005).
- Basov, D. N., Fogler, M. M. & García de Abajo, F. J. Polaritons in van der Waals materials. *Science* **354**, aag1992 (2016).
- Low, T. et al. Polaritons in layered two-dimensional materials. *Nat. Mater.* **16**, 182–194 (2016).
- Novoselov, K. S. et al. Electric field effect in atomically thin carbon films. *Science* **306**, 666–669 (2004).
- Castro Neto, A. H., Guinea, F., Peres, N. M. R., Novoselov, K. S. & Geim, A. K. The electronic properties of graphene. *Rev. Mod. Phys.* **81**, 109–162 (2009).
- Hao, J. et al. High performance optical absorber based on a plasmonic metamaterial. *Appl. Phys. Lett.* **96**, 251104 (2010).
- Lee, C., Wei, X., Kysar, J. W. & Hone, J. Measurement of the elastic properties and intrinsic strength of monolayer graphene. *Science* **321**, 385–388 (2008).
- Balandin, A. A. Thermal properties of graphene and nanostructured carbon materials. *Nat. Mater.* **10**, 569–581 (2011).
- Kane, C. L. & Mele, E. J. Quantum spin Hall effect in graphene. *Phys. Rev. Lett.* **95**, 226801 (2005).
- Wang, Q. H., Kalantar-Zadeh, K., Kis, A., Coleman, J. N. & Strano, M. S. Electronics and optoelectronics of two-dimensional transition metal dichalcogenides. *Nat. Nanotechnol.* **7**, 699–712 (2012).
- Chhowalla, M. et al. The chemistry of two-dimensional layered transition metal dichalcogenide nanosheets. *Nat. Chem.* **5**, 263–275 (2013).
- Evain, M., Brec, R. & Wbango, M. H. Structural and electronic properties of transition metal thiophosphates. *J. Solid State Chem.* **71**, 244–262 (1987).
- Latini, S., Olsen, T. & Thygesen, K. S. Excitons in van der Waals heterostructures: the important role of dielectric screening. *Phys. Rev. B* **92**, 245123 (2015).
- Jariwala, D., Sangwan, V. K., Lauhon, L. J., Marks, T. J. & Hersam, M. C. Emerging device applications for semiconducting two-dimensional transition metal dichalcogenides. *ACS Nano* **8**, 1102–1120 (2014).
- Susner, M. A., Chyasnachyus, M., McGuire, M. A., Ganesh, P. & Maksymovych, P. Metal thio- and selenophosphates as multifunctional van der Waals layered materials. *Adv. Mater.* **29**, 1602852 (2017).
- Überall, H. High-energy interference effect of bremsstrahlung and pair production in crystals. *Phys. Rev.* **103**, 1055–1067 (1956).
- Korobochko, Y. S., Kosmach, V. F. & Mineev, V. I. On coherent electron bremsstrahlung. *Sov. Phys. JETP* **21**, 834–839 (1965).
- Baryshevsky, V. G. & Feranchuk, I. D. Parametric X-rays from ultrarelativistic electrons in a crystal: theory and possibilities of practical utilization. *J. Phys. France* **44**, 913–922 (1983).
- Baryshevsky, V. G., Feranchuk, I. D. & Ulyanenko, A. P. *Parametric X-ray Radiation In Crystals* (Springer, 2005).
- Jiang, P., Qian, X., Gu, X. & Yang, R. Probing anisotropic thermal conductivity of transition metal dichalcogenides MX₂ (M=Mo, W and X=S, Se) using time-domain thermoreflectance. *Adv. Mater.* **29**, 1701068 (2017).
- Zan, R. et al. Control of radiation damage in MoS₂ by graphene encapsulation. *ACS Nano* **7**, 10167–10174 (2013).
- Lehnert, T., Lehtinen, O., Algara-Siller, G. & Kaiser, U. Electron radiation damage mechanisms in 2D MoSe₂. *Appl. Phys. Lett.* **110**, 033106 (2017).
- Kirz, J., Jacobsen, C. & Howells, M. Soft X-ray microscopes and their biological applications. *Q. Rev. Biophys.* **28**, 33–130 (1995).
- de Groot, F. & Kotani, A. *Core Level Spectroscopy of Solids* (CRC Press, 2008).
- Hitchcock, A. P. Soft X-ray spectromicroscopy and ptychography. *J. Electron Spectrosc. Relat. Phenom.* **200**, 49–63 (2015).

26. Agarwal, B. K. *X-ray Spectroscopy: an Introduction* Vol. 15 (Springer, 2013).
27. Hayakawa, Y. et al. X-ray imaging using a tunable coherent X-ray source based on parametric X-ray radiation. *J. Instrum.* **8**, C08001 (2013).
28. Carroll, F. E. Tunable monochromatic X rays: a new paradigm in medicine. *Am. J. Roentgenol.* **179**, 583–590 (2002).
29. Okada, H. et al. Basic study of parametric X-ray radiation for clinical diagnosis using 125 MeV linear particle accelerator. *J. Hard Tissue Biol.* **24**, 299–302 (2015).
30. Saldin, E. L., Schneidmiller, E. A. & Yurkov, M. *The Physics of Free-Electron Lasers* (Springer, 2000).
31. Ackermann, W. et al. Operation of a free-electron laser from the extreme ultraviolet to the water window. *Nat. Photon.* **1**, 336–342 (2007).
32. Winick, H. & Doniach, S. *Synchrotron Radiation Research* (Springer, 2012).
33. Powers, N. D. et al. Quasi-monoenergetic and tunable X-rays from a laser-driven Compton light source. *Nat. Photon.* **8**, 28–31 (2014).
34. Wong, L. J., Kaminer, I., Ilic, O., Joannopoulos, J. D. & Soljačić, M. Towards graphene plasmon-based free-electron infrared to X-ray sources. *Nat. Photon.* **10**, 46–52 (2016).
35. Rosolen, G. et al. Metasurface-based multi-harmonic free-electron light source. *Light Sci. Appl.* **7**, 64 (2018).
36. Pizzi, A. et al. Graphene metamaterials for intense, tunable, and compact extreme ultraviolet and X-ray sources. *Adv. Sci.* **7**, 1901609 (2019).
37. Rivera, N., Wong, L. J., Joannopoulos, J. D., Soljačić, M. & Kaminer, I. Light emission based on nanophotonic vacuum forces. *Nat. Phys.* **15**, 1284–1289 (2019).
38. Blazhevich, S. V. et al. First observation of interference between parametric X-ray and coherent bremsstrahlung. *Phys. Lett. A* **195**, 210–212 (1994).
39. Feranchuk, I. D., Ulyanenko, A., Harada, J. & Spence, J. C. H. Parametric X-ray radiation and coherent bremsstrahlung from nonrelativistic electrons in crystals. *Phys. Rev. E* **62**, 4225–4234 (2000).
40. Fraser, J. S., Sheffield, R. L. & Gray, E. R. A new high-brightness electron injector for free electron lasers driven by RF linacs. *Nucl. Instrum. Methods Phys. Res. A* **250**, 71–76 (1986).
41. Dunham, B. et al. Record high-average current from a high-brightness photoinjector. *Appl. Phys. Lett.* **102**, 034105 (2013).
42. Li, X. et al. Dispersion engineering in metamaterials and metasurfaces. *J. Phys. D* **51**, 054002 (2018).
43. Kaminer, I. et al. Spectrally and spatially resolved Smith–Purcell radiation in plasmonic crystals with short-range disorder. *Phys. Rev. X* **7**, 011003 (2017).
44. Remez, R. et al. Spectral and spatial shaping of Smith–Purcell radiation. *Phys. Rev. A* **96**, 061801 (2017).
45. Geim, A. K. & Grigorieva, I. V. Van der Waals heterostructures. *Nature* **499**, 419–425 (2013).
46. Gjerding, M. N., Petersen, R., Pedersen, T. G., Mortensen, N. A. & Thygesen, K. S. Layered van der Waals crystals with hyperbolic light dispersion. *Nat. Commun.* **8**, 320 (2017).
47. Herman, M. A. & Sitter, H. *Molecular Beam Epitaxy: Fundamentals and Current Status* (Springer, 2012).
48. Dapkus, P. D. Metalorganic chemical vapor deposition. *Annu. Rev. Mater. Sci.* **12**, 243–269 (1982).
49. Graves, W., Kärtner, F., Moncton, D. & Piot, P. Intense superradiant X rays from a compact source using a nanocathode array and emittance exchange. *Phys. Rev. Lett.* **108**, 263904 (2012).
50. Nanni, E. A., Graves, W. S. & Moncton, D. E. Nanomodulated electron beams via electron diffraction and emittance exchange for coherent X-ray generation. *Phys. Rev. Accel. Beams* **21**, 014401 (2018).
51. Naumova, N. et al. Attosecond electron bunches. *Phys. Rev. Lett.* **93**, 195003 (2004).
52. Lim, J., Chong, Y. & Wong, L. J. Terahertz-optical intensity grating for creating high-charge, attosecond electron bunches. *New J. Phys.* **21**, 033020 (2019).
53. Attwood, D. T. *Soft X-Rays and Extreme Ultraviolet Radiation* (Cambridge Univ. Press, 2000).
54. Roessl, E. et al. Sensitivity of photon-counting based K-edge imaging in X-ray computed tomography. *IEEE Trans. Med. Imaging* **30**, 1678–1690 (2011).

Publisher's note Springer Nature remains neutral with regard to jurisdictional claims in published maps and institutional affiliations.

© The Author(s), under exclusive licence to Springer Nature Limited 2020

Methods

Experimental. The radiation was generated by highly collimated electron beams in an FEI Titan Themis G2 TEM with acceleration voltage in the range 60–300 kV, used to control the velocity of the incident electrons. The energy spectrum was measured using a Dual Bruker XFlash 6 | 100 energy-dispersive X-ray spectroscopy detector oriented at $\varphi = 121^\circ$ with respect to the electron velocity vector and with $\Delta\varphi_D = 16^\circ$. The energy resolution of the detector in the energy range of the measurements is ~ 80 eV full-width at half-maximum. The resolution was determined by fitting a Gaussian distribution to the characteristic radiation energy peaks of W and Se in proximity to the PCB radiation peaks. All spectra were obtained by aligning the collimated electron beams along the crystal zone axis ([103] and [001]), verified by their diffraction patterns. The input power in our experiment was of the order of ~ 0.1 mW (~ 100 kV \times 1 nA), much lower than that of commercial X-ray tubes, which lies in the range of tens to thousands of watts. The relatively low input power required relatively long accumulation times of 16 min during the experiment. However, no visible damage was detected on the sample after up to ten such measurements.

Theoretical. The theoretical prediction of the peak emission (vertical dotted lines in Figs. 1d and 2) were obtained using equation (1) without any fitting parameters. We developed two simulation frameworks. In the CBS simulator, the trajectories of the electrons travelling in the vdW material were obtained by solving the relativistic Newton–Lorentz equations using a fifth-order Runge–Kutta algorithm^{34,55}. The impinging electrons were assumed to be normally incident on the plane of the vdW layers. The atomic potential of the vdW material was obtained from DFT computations that take into consideration all inner-shell electrons^{36,57}. The DFT calculations were performed with the GPAW (Grid-based Projector-Augmented Wave) code⁵⁸, which uses a plane-wave basis set to expand the electron wave functions. The radiation from the electrons was calculated from their trajectories via the Liénard–Wiechert formula. Since the electron beam width is far larger than the transverse lattice cell size, the total radiation spectrum was obtained by averaging over the radiation spectra of individual electrons spanning one unit cell of the atomic structure.

In the PXR simulator, the atomic structure was modelled by periodic dipole arrays, and the incident electrons were assumed to travel along straight lines with uniform velocity. The response of the bound electrons around each atom was modelled by effective dipoles, with the atomic polarizability derived from the experimental scattering factor⁵⁹.

The widths of the peaks in Figs. 1 and 2 were calculated by combining ΔE (calculated using equation (2)) with the energy broadening due to the detector energy resolution ΔE_{res} , for an approximate energy width of $\Delta E_{\text{tot}} = \sqrt{\Delta E^2 + \Delta E_{\text{res}}^2}$. The energy widths were also found in another more precise way, using the PXR simulation, and convolving the spectra with a Gaussian (full-width at half-maximum of ΔE_{res}) that models the response of the detector. The results yield the theoretical spectral line presented in Fig. 1. The energy widths obtained in both methods approximate well the experimental data.

Sample preparation. Chromium thiophosphate (CrPS_4) was synthesized by vapour transport synthesis with a temperature gradient of $750^\circ\text{C}/710^\circ\text{C}$ and a reaction time of 4 days, as described in detail elsewhere⁶⁰. Transition metal phosphorous trisulfides were synthesized by the same technique, but the reaction time was longer (1 week), and the temperature gradient was different for each of the specific compounds— MnPS_3 : $650^\circ\text{C}/600^\circ\text{C}$; FePS_3 : $650^\circ\text{C}/550^\circ\text{C}$; CoPS_3 : $625^\circ\text{C}/575^\circ\text{C}$; NiPS_3 : $650^\circ\text{C}/600^\circ\text{C}$. The vdW materials were mechanically exfoliated and directly transferred to a TEM grid using a protocol described in ref. ⁶⁰.

Data availability

The data that support the plots within this paper and other findings of this study are available from the corresponding authors upon reasonable request.

Code availability

The codes that support the plots within this paper and other findings of this study are available from the corresponding authors upon reasonable request.

References

55. Wong, L. J. et al. Laser-induced linear-field particle acceleration in free space. *Sci. Rep.* **7**, 11159 (2017).

56. Wang, W. L. & Kaxiras, E. Efficient calculation of the effective single-particle potential and its application in electron microscopy. *Phys. Rev. B* **87**, 085103 (2013).
57. Susi, T. et al. Efficient first principles simulation of electron scattering factors for transmission electron microscopy. *Ultramicroscopy* **197**, 16–22 (2019).
58. Enkovaara, J. et al. Electronic structure calculations with GPAW: a real-space implementation of the projector augmented-wave method. *J. Phys. Condens. Matter* **22**, 253202 (2010).
59. Henke, B. L., Gullikson, E. M. & Davis, J. C. X-ray interactions: photoabsorption, scattering, transmission, and reflection at $E = 50\text{--}30,000$ eV, $Z = 1\text{--}92$. *At. Data Nucl. Data Tables* **54**, 181–342 (1993).
60. Budniak, A. K. et al. Exfoliated CrPS_4 with promising photoconductivity. *Small* **16**, 1905924 (2020).

Acknowledgements

We thank Y. Kauffmann for advice and discussions. This work was supported by the ERC (Starter Grant no. 851780), the ISF (Grant no. 830/19) and the European Commission via the Marie Skłodowska-Curie Action Phonsi (H2020-MSCA-ITN-642656). H.H.S. also acknowledges the support of Marie Skłodowska-Curie Actions (H2020-MSCA-IF-2018-843830). K.S.T. acknowledges funding from the European Research Council (ERC) under the European Union's Horizon 2020 research and innovation programme (grant no. $\sqrt{73122}$, LIMA). The Center for Nanostructured Graphene is sponsored by the Danish National Research Foundation, Project DNRF103. F.H.L.K. acknowledges financial support from the Government of Catalonia through the SGR grant, and from the Spanish Ministry of Economy and Competitiveness, through the “Severo Ochoa” Programme for Centres of Excellence in R&D (SEV-2015-0522), and Explora Ciencia FIS2017-91599-EXP. F.H.L.K. also acknowledges support by Fundació Cellex Barcelona, Generalitat de Catalunya through the CERCA program, and the Mineco grants Plan Nacional (FIS2016-81044-P) and the Agency for Management of University and Research Grants (AGAUR) 2017 SGR 1656. Furthermore, the research leading to these results has received funding from the European Union's Horizon 2020 under grant agreement no. 785219 (Core2) and no. 881603 (Core3) Graphene Flagship, and no. 820378 (Quantum Flagship). This work was supported by the ERC TOPONANOP under grant agreement no. 726001. L.J.W. acknowledges the support of the Agency for Science, Technology and Research (A*STAR) Advanced Manufacturing and Engineering Young Individual Research Grant (A1984c0043), and the Nanyang Assistant Professorship Start-up Grant. F.J.G.A. acknowledges support from the Spanish MINECO (Grant nos. MAT2017-88492-R and SEV2015-0522), ERC (Advanced Grant no. 789104-eNANO), the Catalan CERCA Program and Fundació Privada Cellex. I.K. was also supported by an Azrieli Faculty Fellowship.

Author contributions

M.S. spearheaded the project, designed and performed the electron microscopy experiments, prepared the samples, analysed the data and developed the superlattice theory. A.K.B. contributed to the measurements and performed electron microscopy experiments. A.K.B., H.H.S., M.B., Y.A., S.T., F.H.L.K. and E.L. synthesized the vdW materials and prepared the TEM samples. R.D. and M.K. advised on experimental aspects. X.S., Y.K. and F.J.G.A. developed and executed the PXR simulations. M.K.S. and K.S.T. performed the DFT simulations. L.J.W. developed and executed the CBS simulations. F.J.G.A., L.J.W., X.S. and I.K. contributed to the discussion of the experimental results, to the comparative analysis of the different theoretical mechanisms and to the overall conclusions. M.S. and I.K. conceived the idea. I.K. supervised the project.

Competing interests

The authors declare no competing interests.

Additional information

Supplementary information is available for this paper at <https://doi.org/10.1038/s41566-020-0689-7>.

Correspondence and requests for materials should be addressed to M.S. or I.K.

Reprints and permissions information is available at www.nature.com/reprints.